Measurement of charged particle yields from therapeutic beams in view of the design of an innovative hadrontherapy dose monitor

2015 JINST 10 C02032

PUBLISHED BY IOP PUBLISHING FOR SISSA MEDIALAB

RECEIVED: *September 21, 2014*
REVISED: *November 6, 2014*
ACCEPTED: *December 15, 2014*
PUBLISHED: *February 18, 2015*

16th INTERNATIONAL WORKSHOP ON RADIATION IMAGING DETECTORS
22–26 JUNE 2014,
TRIESTE, ITALY

Measurement of charged particle yields from therapeutic beams in view of the design of an innovative hadrontherapy dose monitor

G. Battistoni,[c] **F. Bellini,**[a,b] **F. Bini,**[j] **F. Collamati,**[a,b] **F. Collini,**[c] **E. De Lucia,**[d] **M. Durante,**[g] **R.Faccini,**[a,b] **F. Ferroni,**[a,b] **P.M. Frallicciardi,**[f,1] **C. La Tessa,**[g] **M. Marafini,**[f] **I. Mattei,**[h,d] **F. Miraglia,**[a] **S. Morganti,**[b] **P.G. Ortega,**[i] **V. Patera,**[e,b] **L. Piersanti,**[e,b] **D. Pinci,**[b] **A. Russomando,**[a,b] **A. Sarti,**[e,b] **C. Schuy,**[g] **A. Sciubba,**[e,b] **M. Senzacqua,**[a,b] **E. Solfaroli Camillocci,**[k,b] **M. Vanstalle**[g] **and C. Voena**[b]

[a] *Dipartimento di Fisica, La Sapienza Università di Roma, Roma, Italy*
[b] *INFN, Sezione di Roma, Roma, Italy*
[c] *INFN, Sezione di Milano, Milano, Italy*
[d] *Laboratori Nazionali di Frascati dell'INFN, Frascati, Italy*
[e] *Dipartimento di Scienze di Base e Applicate per l'Ingegneria, La Sapienza Università di Roma, Roma, Italy*
[f] *Museo Storico della Fisica e Centro Studi e Ricerche "E. Fermi", Roma, Italy*
[g] *GSI, Darmstadt, Germany*
[h] *Dipartimento di Matematica e Fisica, Roma Tre Università di Roma, Roma, Italy*
[i] *CERN, Geneva, Switzerland*
[j] *Dipartimento di Ingegneria Meccanica e Aerospaziale, Sapienza Università di Roma, Roma, Italy*
[k] *Center for Life Nano Science@Sapienza, Istituto Italiano di Tecnologia, Roma, Italy*

E-mail: paola.frallicciardi@gmail.com

[1] Corresponding author.

doi:10.1088/1748-0221/10/02/C02032

ABSTRACT: Particle Therapy (PT) is an emerging technique, which makes use of charged particles to efficiently cure different kinds of solid tumors. The high precision in the hadrons dose deposition requires an accurate monitoring to prevent the risk of under-dosage of the cancer region or of over-dosage of healthy tissues. Monitoring techniques are currently being developed and are based on the detection of particles produced by the beam interaction into the target, in particular: charged particles, result of target and/or projectile fragmentation, prompt photons coming from nucleus de-excitation and back-to-back γs, produced in the positron annihilation from β+ emitters created in the beam interaction with the target. It has been showed that the hadron beam dose release peak can be spatially correlated with the emission pattern of these secondary particles. Here we report about secondary particles production (charged fragments and prompt γs) performed at different beam and energies that have a particular relevance for PT applications: ^{12}C beam of 80 MeV/u at LNS, ^{12}C beam 220 MeV/u at GSI, and ^{12}C, ^{4}He, ^{16}O beams with energy in the 50–300 MeV/u range at HIT. Finally, a project for a multimodal dose-monitor device exploiting the prompt photons and charged particles emission will be presented.

KEYWORDS: Instrumentation for particle-beam therapy; Control and monitor systems online; Particle tracking detectors; Multi-modality systems

2015 JINST 10 C02032

Contents

1 Introduction

PT is an emerging technique ([1–5]) alternative to conventional radiotherapy (RT), which makes use of charged particles, usually protons and carbon ions, to treat different kinds of solid tumors. Charged particles most attractive feature with respect to the X-rays exploited in RT treatments is their dose profile, showing the highest dose release at the end of their path inside the patient's body, in a region called Bragg Peak (BP). On the other hand the dose released in the entrance region is reduced with respect to the RT, helping to spare the healthy tissues crossed by the beam before the tumor region and, moreover, it is highly suppressed in the region just beyond the BP. The track length is a function of the beam energy, and by using beams of different energies it is possible to accurately conform the dose to the tumor shape (Spread Out Bragg Peak). Moreover carbon ions are characterized by higher LET values with respect to X-rays and thus are more efficient in killing radio-resistant tumours, with a higher Relative Biological Effectiveness (RBE). Due to the ballistic precision of PT, the treatment is extremely sensitive to anatomical changes and patient mis-positioning, with related risk of under-dosage of the cancer region or over-dosage of the healthy tissues. The stringent requirements on the PT dose deposition position control are calling for the development of a high precision on line monitor. Unfortunately, unlike X-rays in conventional RT, the hadron beam is completely absorbed by the body, which implies that it is not possible to use the fraction of the beam escaping from the patient. A promising way to overcome this limitation is to detect secondary particles produced by the beam interaction with patient tissues: charged particles, originating from the projectile and target fragmentation, prompt gammas from nucleus de-excitation, with emission times up to few nanoseconds and pairs of back-to-back photons produced by the annihilation of positrons coming from $\beta+$ emitters generated by the beam interaction with the patient. The dose release peak can be correlated with the emission pattern of these secondary particles ([6–15]).

Several measurements at different hadrontherapy facilities have been performed to measure the correlation of the secondary particles emission pattern with the BP position and their fluxes: (1) at Laboratori Nazionali del Sud (LNS), in Catania (Italy), where both prompt gammas and

charged particles from a PMMA target hit by an 80 MeV/u ^{12}C beam were measured by a detector placed at 90° with respect to the beam incoming direction [16]; (2) at GSI, Darmstadt (Germany), where the same measurements were performed with a beam energy of 220 MeV/u and an additional 60° detection angle configuration [17]; (3) at HIT, Heidelberg (Germany), where energies in the range (50–300) MeV of ^{4}He, ^{12}C and ^{16}O beams were explored in different angular configurations (0°, 10°, 30°, 60°, 90°). Here we present a summary of such measurements, together with the design of a multimodal dose-monitor to be operated at the Centro Nazionale per l'Adroterapia Oncologica (CNAO) in Pavia (Italy). The monitor system will be composed of a two PET heads module, for an online monitoring of the β+ emitters production, and of a dose profiler that will be able to detect, track and measure the energy of both secondary charged particles and prompt gammas, with a spatial resolution of nearly 4 mm for a single pencil beam.

2 Secondary particles detection

2.1 Prompt gammas

Prompt gammas emitted within few nanoseconds by ion beam de-excitations have been detected at LNS facility in Catania (Italy). The ^{12}C, 80 MEV/u beam rate was monitored by a 1.1 mm thick plastic EJ-200 scintillator (used as a start counter, SC), read by two H10580 Hamamatsu photomultiplier tubes (PMT), while a $4 \times 4 \times 4\,\mathrm{cm}^3$ PMMA target was placed on the beam line. An array of 4 LYSO crystals ($1.5 \times 1.5 \times 12\,\mathrm{cm}^3$ each) was placed at 90° with respect to the beam line. The scintillation light of the crystals was detected with an EMI 9814B PMT triggered in coincidence with the SC. This setup allowed the discrimination of prompt gammas from the non-relativistic neutrons background.

Figure 1 (left) shows the neutral particles energy as a function of the time difference, ΔT, between the LYSO crystal and the SC, corrected for the time slewing effect that takes into account the different times needed to cross the discrimination thresholds by signals with different amplitude. Figure 1 (right) shows the measured spectrum, background subtracted, normalized to the number of incident carbon ions and corrected for the dead time inefficiency. The peak visible in the spectrum near 4 MeV comes from the ^{12}C* de-excitation line.

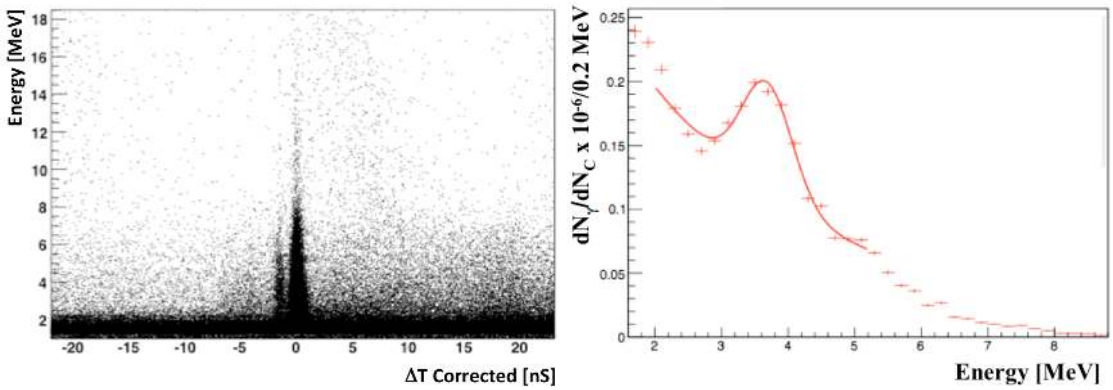

Figure 1. Energy released in LYSO crystal as a function of the arrival time (left); prompt gammas energy spectrum obtained with the LYSO detector (right).

The measured differential production rate, above 2 MeV, per number of carbon ions, N_c and solid angle, Ω, has been evaluated as:

$$\frac{dN_\gamma}{dN_C d\Omega}(E > 2\,\mathrm{MeV}, \vartheta = 90^\circ) = (2.32 \pm 0.01_{\mathrm{stat}} \pm 0.15_{\mathrm{sys}}) \times 10^{-3} sr^{-1} \tag{2.1}$$

Evidence of prompt gammas detected at 60° and 90° has been found also with ^{4}He and ^{16}O beams at HIT facility. Data from these measurements have still to be analysed and the results showed below are just preliminary. Figure 2 shows raw charge-to-digital converted (QDC) counts as a function of ΔT distribution, for a 125 MeV/u ^{4}He beam.

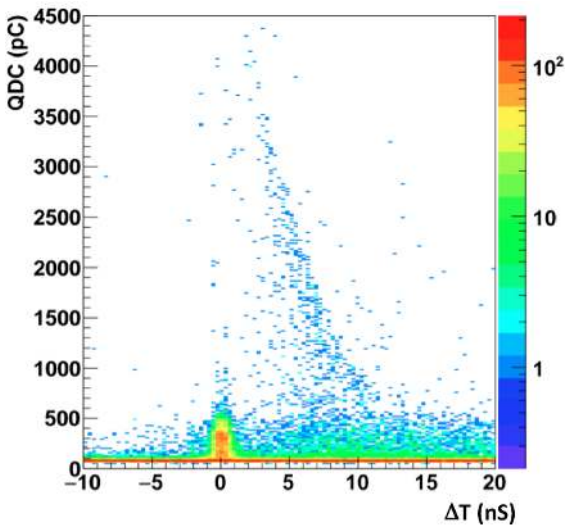

Figure 2. Preliminary raw data, charge-to-digital converted (QDC) counts vs ΔT, showing evidence of gammas prompt emission detected at 90° from a PMMA target hit by a 125 MeV/u ^{4}He beam. A small peak due to prompt gammas is clearly visible at $\Delta T \sim 0$ as well as a band populated by protons at higher ΔT and QDC values.

The gammas prompt peak at ΔT values approximately zero and low QDC counts number (left in the figure) is clearly visible together with the protons band at higher ΔT values and QDC counts (right in the figure), where ΔT represents the time of flight measured from the SC to the LYSO.

2.2 Charged particles

To measure the charged particles component emitted by the LNS 80 MeV/u ^{12}C beam, the setup previously described was integrated with a drift chamber (DC) between the PMMA target and the LYSO detector, to track ions from the detector back to the production region inside the target.

The charged particles emitted at 90° with respect to the beam incoming direction have a flux that is highly reduced when compared to the forward production (around 0°) but, on the other side, they have to travel a smaller path inside the PMMA phantom and hence suffer for a reduced multiple scattering. The improvement in the spatial resolution achievable on the emission point pairs with the need, from the MC community, to have a good experimental description of the large angle emission of charged fragments that is currently poorly reproduced by the simulations are the reason why a 90° geometrical setup has been used to study the charged particles production in the

different experimental sites. Figure 3 (left) shows, the experimental distribution of the emission points of protons inside the PMMA, obtained for all charged particles identified as protons and for protons with different kinetic energy ($E_{kin} > 60$ MeV and $E_{kin} > 100$ MeV). The separation between the BP and the peak from the secondary protons emission has been evaluated as $\Delta_{ProtonBragg} = 8.1\,mm \pm 0.5\,mm$: such measurement proves the BP monitoring capability of a charged particles based monitoring technique. To demonstrate the linear relationship between the x-position of the BP and the mean x-position value of the distribution of secondary particles emission point, a linear position scan of the PMMA target along the beam direction was done. Figure 3 (right) shows how the peak x-coordinate of the charged emission follows the movement of the target, and hence of the BP position, along the beam direction (x_{PMMA} coordinate). Since y_{PMMA} is the coordinate of the proton emission point along the vertical axis, and it is related to the fixed beam profile in the transverse plane, it remains constant with respect to the BP abscissa, x_{Bragg}, and it provides an estimate of the method's systematic uncertainty. The backtracking of the charged secondary particles allows measuring the BP position with a resolution $\sigma_{Emission}$ of ≈ 0.7 mm, evaluated as:

$$\sigma_{Emission} = \sqrt{\sigma^2_{\Delta ProtonBragg} - \sigma^2_{Extrapol} - \sigma^2_{Stage}}\,,$$

where: $\sigma_{Extrapol} = 0.5$ mm is due to the backward extrapolation of the track from the drift chamber to the beam line (and can be evaluated as σ_{yPMMA}), $\sigma_{\Delta ProtonBragg} \approx 0.9$ mm is the root mean square of $\Delta_{ProtonBragg}$ and $\sigma_{Stage} = 0.2$ mm is the uncertainty on the PMMA positioning.

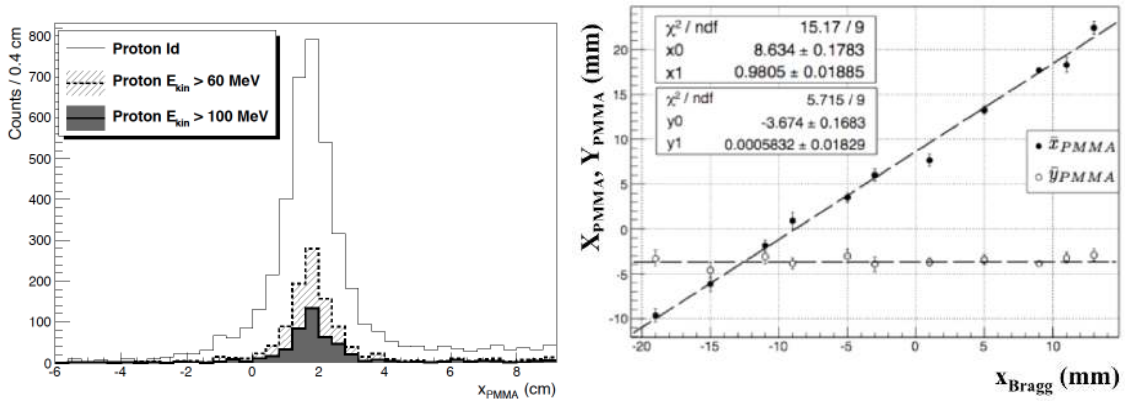

Figure 3. Distribution of the emission points (longitudinal emission profile) of secondary charged particles (solid) along the beam x-axis, x_{PMMA} for all particles identified as protons (solid line), for protons with kinetic energy threshold $E_{kin} > 60$ MeV (dashed line) and with $E_{kin} > 100$ MeV (gray); the beam entrance and exit faces of the PMMA are at $x_{PMMA} = 2$ cm and $x_{PMMA} = -2$ cm, respectively (left); reconstructed peak position of the secondary proton emission distribution x_{PMMA}, y_{PMMA} as a function of the expected BP position x_{Bragg}, for protons with kinetic energy $E_{kin} > 60$ MeV (right).

The flux of the secondary protons measured at 90° with respect to the beam direction with kinetic energy $E_{kin} > 83$ MeV (kinetic energy threshold for a proton capable of escaping a 5 cm deep tumor accordingly to the FLUKA ([16, 17]) MC simulation software), normalized to the number of incoming carbon ions, N_C, and detector solid angle, Ω, is:

$$\frac{dN_P}{dN_C d\Omega}(E > 83\,\mathrm{MeV}, \vartheta = 90^\circ) = (0.214 \pm 0.006_{stat} \pm 0.010_{sys}) \times 10^{-4} sr^{-1} \qquad (2.2)$$

2015 JINST 10 C02032

The same experimental setup was exploited in GSI with a 220 MeV/u ^{12}C beam, where an additional measurement was performed at an angle of 60° with respect to the beam direction. The PMMA target dimensions were of $20 \times 5 \times 5\,\mathrm{cm}^3$. Evidence of protons, deuterons and tritons from both 60° and 90° angles is shown in figure 4 (left and right, respectively), in which the three bands are clearly visible.

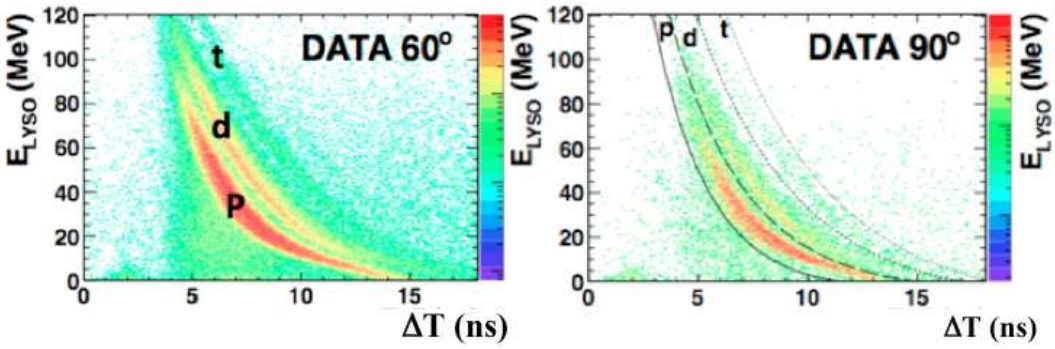

Figure 4. Data distributions of the released energy in the LYSO detector, E_{LYSO}, as a function of the ΔT for the 60° (left) and 90° (right) setup. Protons, deuterons and tritons bands are clearly visible.

Measured fluxes, normalized to the number of incoming carbon ions, N_C, and detector solid angle, Ω, are:

$$\frac{dN_p}{dN_C d\Omega}(\vartheta = 60^\circ) = (8.78 \pm 0.07_{\mathrm{stat}} \pm 0.64_{\mathrm{sys}}) \times 10^{-3} sr^{-1}$$
$$\frac{dN_d}{dN_C d\Omega}(\vartheta = 60^\circ) = (3.71 \pm 0.04_{\mathrm{stat}} \pm 0.37_{\mathrm{sys}}) \times 10^{-3} sr^{-1}$$
$$\frac{dN_t}{dN_C d\Omega}(\vartheta = 60^\circ) = (0.91 \pm 0.071 \pm 0.21_{\mathrm{sys}}) \times 10^{-3} sr^{-1}$$
$$\frac{dN_p}{dN_C d\Omega}(\vartheta = 90^\circ) = (1.83 \pm 0.02_{\mathrm{stat}} \pm 0.14_{\mathrm{sys}}) \times 10^{-3} sr^{-1}$$
$$\frac{dN_d}{dN_C d\Omega}(\vartheta = 90^\circ) = (0.78 \pm 0.01_{\mathrm{stat}} \pm 0.09_{\mathrm{sys}}) \times 10^{-3} sr^{-1}$$
$$\frac{dN_t}{dN_C d\Omega}(\vartheta = 90^\circ) = (0.128 \pm 0.005_{\mathrm{stat}} \pm 0.028_{\mathrm{sys}}) \times 10^{-3} sr^{-1}.$$

The charged secondary fragments spatial distribution (figure 5 (a)) is clearly linked to the BP position and it is hence possible to correlate the parameters of an analytical function that describes the measured spectrum to its position, as shown in figure5 (b). The Δ_{40} parameter represents the width of the distribution at 40% of its maximum, X_{left} and X_{right} are the values at rising and falling edges, respectively, and δ_{40} is the distance between X_{left} and the x-intercept of the tangent to the distribution at $X = X_{\mathrm{right}}$. X_{left} can be related to the position of the patient during a treatment that is crucial information for dose monitoring. The parameters measured resolutions are listed in figure 5 (c), and are relative to a sample of 10^3 charged secondary particles corresponding approximately to one pencil beam for a standard treatment. The accuracy achievable on the position of one tumor slice treated with a number N_{Beams} of pencil beams will, hence, be sub millimetric.

Figure 6 shows a preliminary result obtained at HIT facility (Heidelberg, Germany), where protons, deuterons and tritons, produced by a 125 MeV/u ^{4}He beam impinging on a PMMA target, were detected at 0°, 60° and 90°. The distribution shown in figure 6 is relative to the 0° configuration; the three bands are clearly visible in the QDC, ΔT plane.

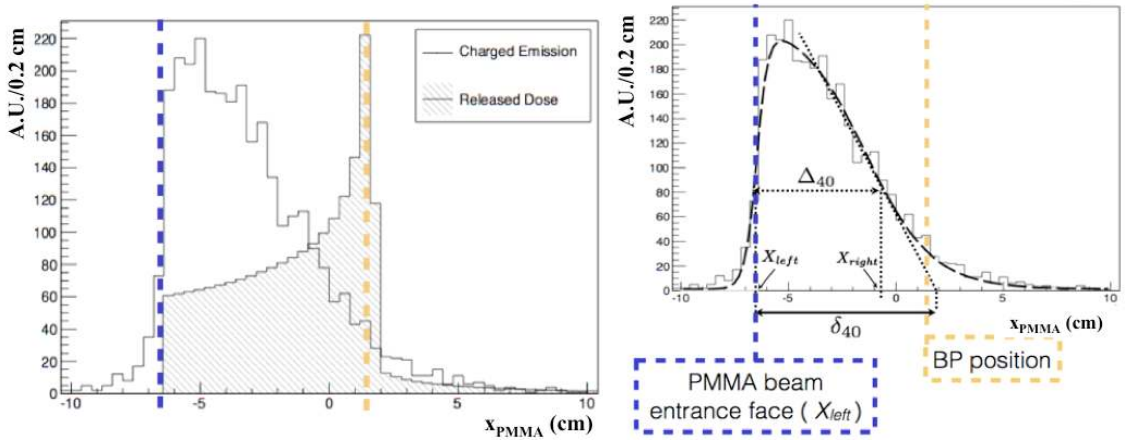

(a) (b)

Angle (deg)	σ_Δ (cm)	σ_δ (cm)	$\sigma_{X_{left}}$ (cm)	$\overline{\Delta_{40}}$ (cm)	$\overline{\delta_{40}}$ (cm)
90	0.34	0.37	0.08	6.60 ± 0.09	9.40 ± 0.10
60	0.31	0.28	0.09	6.83 ± 0.03	9.44 ± 0.03

(c)

Figure 5. Comparison between the FLUKA simulated dose distribution (hatched) superimposed to the longitudinal profile (solid line) of charged secondary particles (a) and parameterization of the profile, linked to the BP position (b). In blue it is highlighted the position of the PMMA entrance face of the beam, while in yellow it is indicated the BP abscissa position (both in (a) and in (b)); resolutions $\sigma(\Delta_{40})$, $\sigma(\delta_{40})$ and $\sigma(X_{left})$, for each angular configurations, are evaluated as the RMS of the measured distributions (c).

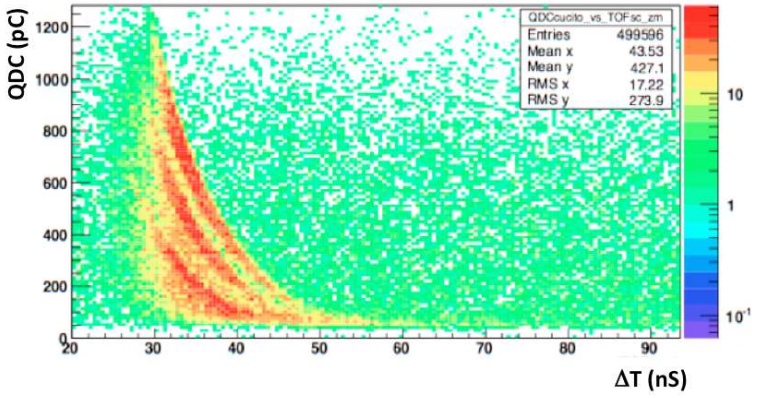

Figure 6. Preliminary data distributions of the raw QDC charge as a function of the ΔT (ns) detected by a BGO detector at 0° after the PMMA phantom hit by a 125 MeV/u ^{4}He beam. Protons, deuterons and tritons bands are clearly visible.

3 Multimodal dose monitor

The INSIDE (Innovative Solutions for In-beam Dosimetry in hadrontherapy) project is born from the collaboration of a number of Italian Universities (Pisa, Rome, Turin, and Politecnico di Bari) and INFN to build a multimodal in-beam dose monitor that will be able to detect at the same time, back-to-back gammas from $\beta+$ annihilation (not covered in this contribution), charged secondary particles emerging from the patient and prompt gammas with energies higher than 1 MeV. The monitor layout foresees of a couple of $10 \times 20\,\mathrm{cm}^2$ PET heads for back-to-back gammas detection and a $20 \times 20\,\mathrm{cm}^2$ dual-mode dose profiler made of 3 sub-detectors: a tracker, an absorber and a calorimeter. The profiler aim is the simultaneous detection and back-tracking of charged particles and prompt gammas (reconstructing the Compton scattering). Figure 7 shows the two working principles for charge and neutral particles detection.

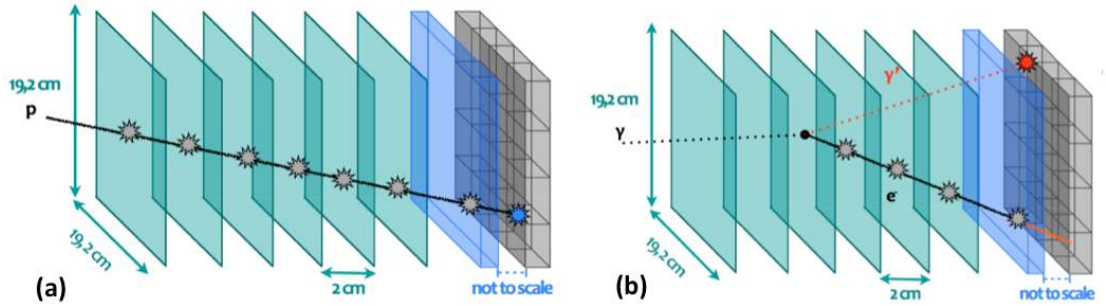

Figure 7. Working principle of the dose profiler for tracking and retrieve energy information on charge particles (mainly protons) (a) and prompt gammas (b).

The tracker will be made of 6 XY planes of 384 ($0.5 \times 0.5\,\mathrm{mm}^2$) BCF-12 plastic scintillating fibers, read out by S12571-050 Hamamatsu 1 mm^2 SiPM coupled to a 32 channel custom ASIC BASIC32 ADC. Behind the tracker, a 2.4 cm thick EJ-200 plastic scintillator slab will be positioned to absorb and measure the energy of Compton electrons. Finally a calorimeter, made of 4×4 matrices of scintillating pixelated LYSO crystals, will detect and measure the energy of Compton gammas and charged particles. Each matrix is made of a 16×16 array of 2 cm thick LYSO that are read by a multianode H8500 PMT. The profiler geometrical layout and the corresponding hardware technology have been optimized using a full FLUKA MC simulation of a PT treatment in which the secondary particles measurements presented in this contribution were implemented. The multimodal dose monitor is nowadays under construction and will be tested at CNAO center.

4 Discussion and conclusion

Quality control in PT treatments needs new devices for on-line dose monitoring. We presented here a multi-modal device, composed of two PET heads and a dose profiler thought to operate simultaneously as a charged particle tracker and to reconstruct Compton events from prompt gammas. To develop this device we performed a set of measurements of yields, emission points distribution and energy spectrum of the secondary charged and neutral particles produced by the therapeutic beam interacting with a PMMA phantom. The geometrical and physical detector parameters have been optimized by an accurate MC simulation based on such measurements results. The achievable

spatial resolution to localize the BP position, related to the charged particle spatial resolution has been evaluated less than 4 mm for one pencil beam. Aiming at the detection of the position of a tumor slice treated with a number N_{Beams} of pencil beams, this result must by divided by $\sqrt{N_{Beams}}$, thus achieving the sub-millimeter range.

We aknowledge the Grant Agreement n 228436 of the FP7 European Program for the data taking at the HIT facility.

References

[1] O. Jäkel et al., *The future of heavy ion therapy*, *Med. Phys.* **35** (2008) 5653.

[2] M. Durante and J.S. Loeffler, *Charged particles in radiation oncology*, *Nat. Rev. Clin. Oncol.* **7** (2010) 37.

[3] U. Amaldi and G. Kraft, *Radiotherapy with beams of carbon ions*, *Rep. Prog. Phys.* **68** (2005) 1861.

[4] D. Schardt et al., *Heavy-ion tumour therapy: physical and radiobiological benefits*, *Rev. Mod. Phys.* **82** (2010) 383.

[5] A. Brahme, *Optimal use of light ions for hadrontherapy*, in *NIRST Symp. On Radiation Life Science* (1986), pg. 18.

[6] E. Testa et al., *Dose Profile monitoring with carbon ions by means of prompt-gamma measurements*, *Nucl. Instrum. Meth.* **B 267** (2009) 993.

[7] C.H. Min et al., *Prompt gamma measurements for locating the dose falloff region in the proton therapy*, *Appl. Phys. Lett.* **89** (2006) 183517.

[8] W. Enghard et al., *Charged hadron tumour monitoring by means of PET*, *Nucl. Instrum. Meth.* **A 525** (2004) 284.

[9] F. Fiedler et al., *In beam PET measurements of biological half-lives of ^{12}C irradiation induced $\beta+$ activity*, *Acta Oncol.* **47** (2008) 1077.

[10] K. Parodi et al., *In-beam PET measurements of $\beta+$ radioactivity induced by proton beams*, *Phys. Med. Biol.* **47** (2002) 21.

[11] F. Attanasi, *Comparison of two dedicated 'in-beam' PET systems via simultaneous imaging of ^{12}C-induced β^+-activity*, *Phys. Med. Biol.* **54** (2009) N29.

[12] C. Agodi et al., *Study of the time and space distribution of β^+ emitters from 80 MeV/u carbon ion beam irradiation on PMMA*, *Nucl. Instrum. Meth.* **B 283** (2012) 1 [arXiv:1202.1676].

[13] C. Agodi et al., *Precise measurements of prompt photon emission for carbon ion therapy*, 2012 *JINST* **7** P03001.

[14] C. Agodi et al., *Erratum: Precise measurement of prompt photon emission from 80 MeV/u carbon ion beam irradiation*, 2013 *JINST* **8** E11002.

[15] F. Bellini et al., *Extended calibration range for prompt photon emission in ion beam irradiation*, *Nucl. Instrum. Meth.* **A 745** (2014) 114.

[16] C. Agodi, *Charged particle's flux measurement from PMMA irradiated by 80 MeV/u carbon ion beam*, *Phys. Med. Biol.* **57** (2012) 5667.

[17] L. Piersanti, *Measurements of charged particles yield from PMMA irradiated by 220 MeV/u ^{12}C beam*, *Phys. Med. Biol.* **59** 1857.

[18] G. Battistoni et al., *The FLUKA code: description and benchmarking*, *AIP Conf. Proc.* **896** (2006) 31.

[19] A. Ferrari et al., *Fluka: a multiple particle transport code*, CERN-2005-010, INFN-TC-2005-11 (2005).